SURFACE DEFORMATION MONITORING IN TUNNEL S2 OF THE EGNATIA HIGHWAY

Dr. Spiros Karamitsos
Email: karamits@central.ntua.gr

Mr. Ioannis Kotsis
Topomet S.A.- School of Rural and Surveying Engineering
National Technical University of Athens
Email: jkotsis@survey.ntua.gr

Dr. Vassilis Gikas
School of Rural and Surveying Engineering
National Technical University of Athens
Email: vgikas@central.ntua.gr

Mr. Andreas Alivizatos
Email: and60@panafonet.gr

Abstract: This paper presents the work which was carried out in order to detect, monitor and model the surface deformations encountered during the excavation of tunnel S2 of the Egnatia highway, which is currently under construction. The Egnatia highway is one of the most significant motorway projects undertaken in Greece, crossing the north of the country from west to east through vast mountainous regions of Epirus. The varying ground conditions in the tunnel S2 area were resulted in slope stability problems during excavation, which realized in the form of severe horizontal and vertical deformations as well as collapses at the crown. The geodetic work combined with drill inclinometer measurements revealed major deformations, both horizontally and vertically. The severity of the deformations is indicated by their magnitude, which is in the order of 1.2 cm/month and 0.8 cm/month for the planimetric and vertical components respectively, as well as by the fact of the partial collapses of the tunnel's interior portion and face entrance. In this paper, the full extend of the geodetic measurements and processing work as well as an attempt to model the kinematics of the derived data is discussed. Also, a set of criteria for the acceptance of the validity of the derived horizontal motions and settlements is proposed.

1. BACKGROUND

Tunnel S2 of the Egnatia highway is located in the western zone of the motorway some 35 km from Igoumenitsa Port. It is a twin tunnel with two lanes per branch and approximate length of 1 km. The overburden of the tunnel is relatively low, ranging from approximately 3 to 60 m. The tunnel passes through a variety of geologic formations consisting of limestone of variable geotechnical characteristics, sheared slickensided sediments and quaternary screes.

The weak soils called for extensive support measures such as dense fore polling umbrellas 12 m long with an overlap of 4 m [1, 2].

The geologic features of the area have been causing problems since the very beginning of the project, mainly in the shape of slope instability at the area of the south portal. Serious problems also occurred during the summer of 2005; at this time extreme convergence values were observed and severe collapses in the interior and temporary retaining measure failures were occurred. These problems were also evident on the surface of the ground in the area above and near the portals, which realized in the form of cracks and numerous fractures. The linkup of these problems, called for the monitoring effort which began in the July of 2005 and ended in September of the same year. The monitoring project was included terrestrial (geometrical leveling) and satellite (GPS) geodetic methods, inclinometer measurements and the installation of number of crack-meters.

2. NETWORK DESIGN, SETUP AND MEASUREMENTS

The monitoring network comprises a total of 18 target points (M01-M16 and M20-M21) located at the overburden region near the south portals of the tunnels, and of three reference points (T7A, T9A and T2) established far beyond the influence zone. The target points cover a small area of approximately 8000 m^2 (roughly 140 m x 140 m) – see Figure 2, while the three reference points were placed in different directions and in distances ranging from 500 m to 1500 m from the test site area; thus, it can be adequately assumed that they lie far out of the deformation zone. It is worth to note that the monitoring network covers only the southern portion of the project area. Most of the target points have been established closely above the two branches of the tunnel, whereas, the rest of them have been placed uphill to the west, from were the main trend of the deformation was expected to occur.

Horizontal displacements were computed by means of static GPS positioning, while point subsidence was measured by means of high precision leveling. The field procedures adopted in this study assumed that a redundant number of reference points were observed at every epoch of measurements. The reason for this is twofold. Firstly, in order to indemnify field work in the event that a reference point was damaged or lost. Secondly, in order to verify the hypothesis that the reference points do not relate to the kinematics of the deformation area. It is noted that only one of the reference points was kept fixed for the purpose of network adjustment. The stability of the reference points was verified by adjusting independently the elementary network formed by these points with the minimal external constrains (i.e., one position held fixed) in every epoch the entire network was surveyed.

The network apexes were materialized by means of concrete pillars of approximately 0.60 m height, equipped with forced centering installations in order to ensure instrument setup error minimization. The relatively short monument height was adopted in order to facilitate geometrical leveling. The GPS recording interval in every survey was set to 10 sec and the duration of the measurements ranged from 3 to 6 hours for every baseline. The baseline solution was derived directly from the L1 carrier phase measurements due to the short baseline length. The vertical deformation was monitored by two-way high precision geometrical leveling, using InVar rods.

3. DATA PROCESSING

All baselines were processed using the double differences of the L1 carrier phases. Due to excessive vegetation in many target points (M04, M09, M12 and M13), editing of the

observations and a carefully selected value of elevation cutoff angle deemed to be necessary. The following requirements were set in order to accept a baseline solution:

- successful integer ambiguity resolution with a ratio higher than 6,
- RMS error of the observations not higher that 0.010 m,
- maximum reference variance value of 16, and
- successful baseline loop closures, i.e. 1 cm horizontally and 3 cm in height.

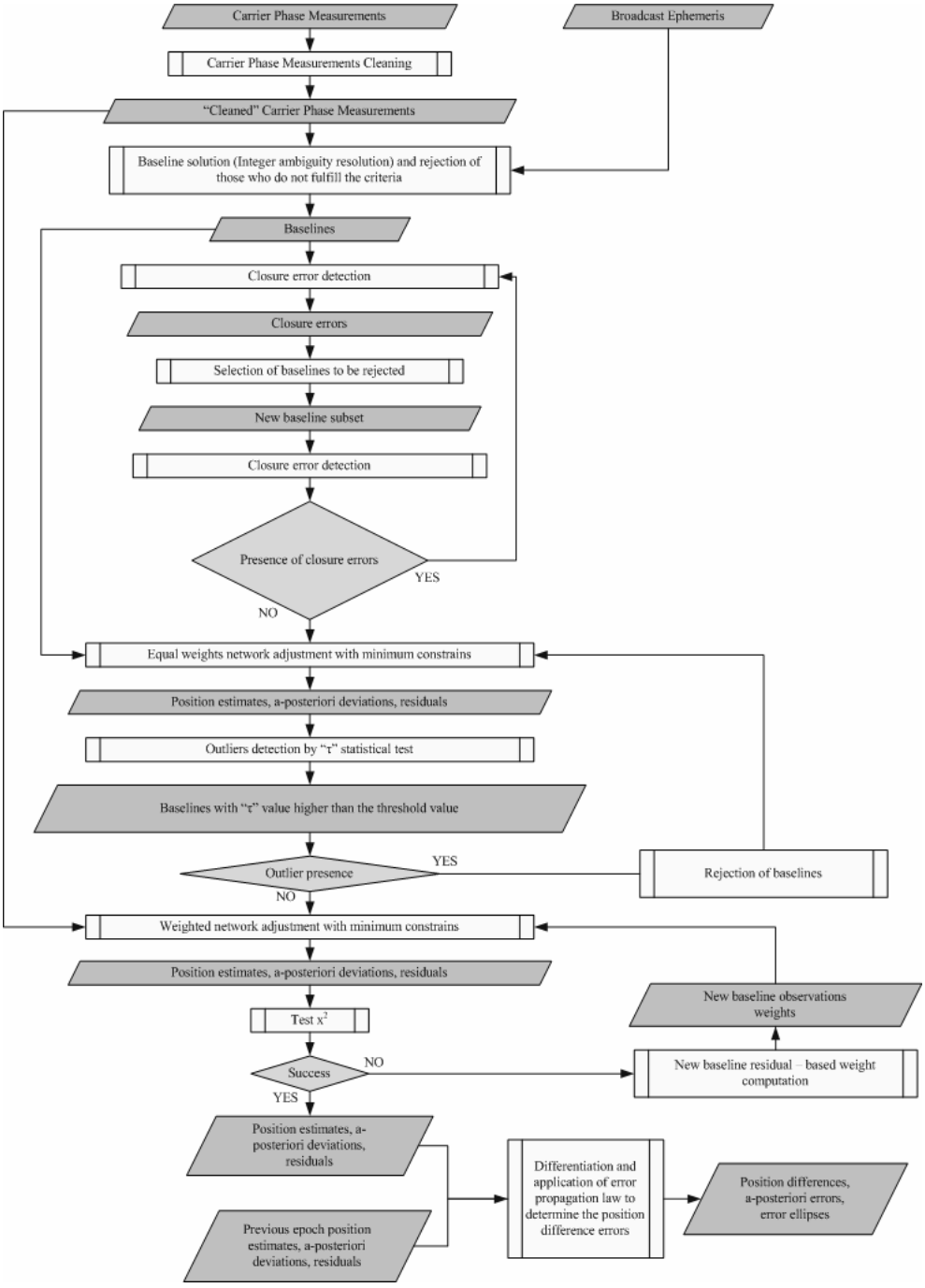

Figure 1: Flowchart outline of GPS data processing scheme.

In order to maintain the expected high internal accuracy of the surveyed network the adjustment of the network comprising the resolved baselines was carried out with the minimal external constraints. Therefore, no known coordinates were imported as constraints for any

apex of the network. The unique constraint was an approximate conventional position of one of the reference points (T9A) in WGS-84, held fixed for all observation epochs. The remaining two reference points were included in the network, simply, in order to further increase the network's degrees of freedom and to enable the uninterrupted continuation of the monitoring in the event that the reference point was damaged or lost.

Data processing was split in a number of distinct steps. In the first step, in order to detect for outlying observations (baselines) an adjustment with equal weights was executed followed by the t-test for the ratio of the residuals to their a-posteriori deviation (v/σ_v) according to the Student distribution. After the baselines have been cleaned, a series of consecutive weighted least squares adjustments were carried out, the weights for each observation baseline being computed from their residuals values of the previous adjustment. Consequently, every adjustment was followed by a chi-square test for the ratio between the a-priori and the a-posteriori variance unit. Failure in this test dictated the alteration of the a-priori value of the weight unit, and execution of an additional adjustment. This process was deemed to conclude upon the chi-square test was succeed. The position differences of the target points between observation epochs were computed by calculating the differences of their respective positions in WGS-84, and then, by converting them into local geodetic position differences (Delta East, Delta North, Delta Up). More specifically, the position difference vectors between the two epochs are computed by:

$$\begin{bmatrix} \Delta X_i^{10} \\ \Delta Y_i^{10} \\ \Delta Z_i^{10} \end{bmatrix} = \begin{bmatrix} X_i^1 \\ Y_i^1 \\ Z_i^1 \end{bmatrix} - \begin{bmatrix} X_i^0 \\ Y_i^0 \\ Z_i^0 \end{bmatrix} \tag{1}$$

Simple application of the variance-covariance law of propagation leads to the computation of the error estimates of the position differences, given by:

$$\begin{bmatrix} \sigma^2_{\Delta X_i} & \sigma_{\Delta X_i \Delta Y_i} & \sigma_{\Delta X_i \Delta Z_i} \\ \sigma_{\Delta X_i \Delta Y_i} & \sigma^2_{\Delta Y_i} & \sigma_{\Delta Y_i \Delta Z_i} \\ \sigma_{\Delta X_i \Delta Z_i} & \sigma_{\Delta Y_i \Delta Z_i} & \sigma^2_{\Delta Z_i} \end{bmatrix} =$$

$$= \begin{bmatrix} 1 & 0 & 0 & -1 & 0 & 0 \\ 0 & 1 & 0 & 0 & -1 & 0 \\ 0 & 0 & 1 & 0 & 0 & -1 \end{bmatrix} \begin{bmatrix} \sigma^2_{X_i^1} & \sigma_{X_i^1 Y_i^1} & \sigma_{X_i^1 Z_i^1} & 0 & 0 & 0 \\ \sigma_{X_i^1 Y_i^1} & \sigma^2_{Y_i^1} & \sigma_{Y_i^1 Z_i^1} & 0 & 0 & 0 \\ \sigma_{X_i^1 Z_i^1} & \sigma_{Y_i^1 Z_i^1} & \sigma^2_{Z_i^1} & 0 & 0 & 0 \\ 0 & 0 & 0 & \sigma^2_{X_i^0} & \sigma_{X_i^0 Y_i^0} & \sigma_{X_i^0 Z_i^0} \\ 0 & 0 & 0 & \sigma_{X_i^0 Y_i^0} & \sigma^2_{Y_i^0} & \sigma_{Y_i^0 Z_i^0} \\ 0 & 0 & 0 & \sigma_{X_i^0 Z_i^0} & \sigma_{Y_i^0 Z_i^0} & \sigma^2_{Z_i^0} \end{bmatrix} \begin{bmatrix} 1 & 0 & 0 & -1 & 0 & 0 \\ 0 & 1 & 0 & 0 & -1 & 0 \\ 0 & 0 & 1 & 0 & 0 & -1 \end{bmatrix}^T \tag{2}$$

Finally, the earth-centered, earth-fixed position differences and of their corresponding variance and covariance values are converted to the local geodetic reference system as follows:

$$\begin{bmatrix} \Delta N_i^{10} \\ \Delta E_i^{10} \\ \Delta U_i^{10} \end{bmatrix} = R(\varphi_i,\lambda_i) \begin{bmatrix} \Delta X_i^{10} \\ \Delta Y_i^{10} \\ \Delta Z_i^{10} \end{bmatrix} \tag{3}$$

where, **R** is the rotation matrix between the two coordinate systems. Finally, the variance covariance matrix of the position differences in the local geodetic reference system is given by:

$$\begin{bmatrix} \sigma^2_{\Delta N_i} & \sigma_{\Delta N_i \Delta E_i} & \sigma_{\Delta E_i \Delta U_i} \\ \sigma_{\Delta N_i \Delta E_i} & \sigma^2_{\Delta E_i} & \sigma_{\Delta E_i \Delta U_i} \\ \sigma_{\Delta E_i \Delta U_i} & \sigma_{\Delta E_i \Delta U_i} & \sigma^2_{\Delta U_i} \end{bmatrix} = \mathbf{R}(\varphi_i, \lambda_i) \begin{bmatrix} \sigma^2_{\Delta X_i} & \sigma_{\Delta X_i \Delta Y_i} & \sigma_{\Delta X_i \Delta Z_i} \\ \sigma_{\Delta X_i \Delta Y_i} & \sigma^2_{\Delta Y_i} & \sigma_{\Delta Y_i \Delta Z_i} \\ \sigma_{\Delta X_i \Delta Z_i} & \sigma_{\Delta Y_i \Delta Z_i} & \sigma^2_{\Delta Z_i} \end{bmatrix} \mathbf{R}^T(\varphi_i, \lambda_i) \tag{4}$$

The processing steps detailed in this Section are summarized in Figure 1.

4. DISCUSSION ON THE RESULTING POSITION DIFFERENCES

Between 11/07/2005 and 09/09/2005 eleven epochs of measurements were taken resulting to nearly nine weeks total period of continuous observations. Deformation analysis was carried out separately for plane coordinates and height differences based on the GPS and precise leveling observations respectively. Figure 2 and Table 1 display the results of the deformation analysis obtained between the first and the 11th epoch. In Figure 2 the horizontal displacements are represented by the difference vectors with error ellipses pinpointed at their start points. Two points are immediately evident from this diagram. First, the mean displacement observed in the landslide area for the entire period of observations is of the order of 2.4 cm representing and average velocity of movement of 1.2 cm/month. Moreover, it is important to point out that the values quoted in Table 1 represent actual movement of the geodetic stations in question; that is to say, the deformation vectors are statistically significant indeed. As can be seen from Figure 2 and Table 1 most of the displacement vectors are clearly jut out from their error ellipses constructed at a confidence level of 99%. The second point to note from this diagram is that the general direction of movement in the horizontal plane exhibits both a strong correlation with topography and a general east, north-east trend. However, a more detailed examination of Figure 2 reveals kinematic heterogeneities in the landslide body which identify zones affected by different superficial activity. More specifically, the deformation analysis was led to a classification of three groups of horizontal motions, confirming the geologic fault pattern shown in Figure 2.

The central part of the landslide (points M01, M04, M05, M07, M08, M09, M10, M12, M13, M14 and M15 - sector A) reveals higher rates of displacement compared with other sectors in the test site. All stations in sector A present statistically significant displacements with a notable correlation in the direction of movement. More specifically, a clear trend of movement can be observed, that follows the topography of the slope. However, if Figure 2 is examined more carefully, it is evident that this directional trend (with an exemption of point M07) is biased to north-east, indicating a tendency the ground stations to shift towards the tunnel bores under construction. This observation is discussed in more detail in Section 5.

The displacement of points M16, M20 and M21 (sector B) is rather irregular with almost no significant motion to be taken into account. The lower activity of these points illustrates the

fact that this group of nodes is located in the area surrounding the south end of the tunnel tubes. It is realized that, in this area the effect of excavation works on ground displacements is expected to be minimum. Also, from Figure 2 it is evident that points M02, M03 and M06 (sector C) do not follow the general trends observed for the points of sector A. In this connection a possible reason may be the geologic discontinuities identified in the south western flank of the area. This was verified independently by the establishment and monitoring of a number of crack-meters in the test site. Moreover, it is possible that inconsequent and of a local character movements may contribute in this kinematic behavior.

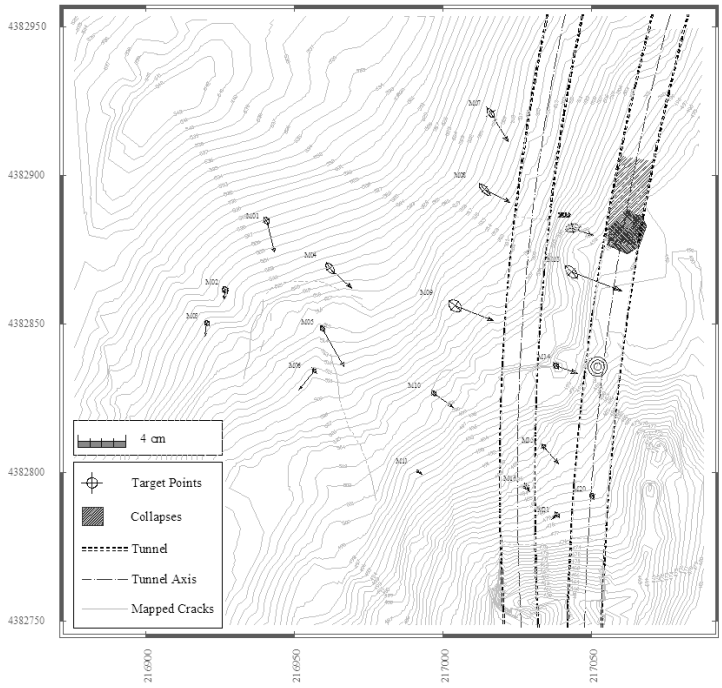

Figure 2: Horizontal displacement vectors with their confidence ellipses (0.99) for the period 11/07/2005 - 09/09/2005.

ID	Position Differences			Position Differences Errors		
	Delta E (m)	Delta N (m)	Delta Hgt (m)	$\sigma_{Delta\ E}$ (m)	$\sigma_{Delta\ N}$ (m)	$\sigma_{Delta\ Hgt}$ (m)
M01	0.0066	-0.0264	-0.0171	0.0023	0.0027	0.0166
M02	-0.0008	-0.0080	-0.0002	0.0023	0.0025	0.0186
M03	-0.0014	-0.0112	-0.0020	0.0018	0.0020	0.0140
M04	0.0180	-0.0167	-0.0171	0.0036	0.0044	0.0234
M05	0.0180	-0.0319	-0.0238	0.0019	0.0021	0.0149
M06	-0.0127	-0.0163	-0.0121	0.0018	0.0019	0.0136
M07	0.0144	-0.0241	-0.0120	0.0031	0.0037	0.0127
M08	0.0214	-0.0105	-0.0193	0.0045	0.0048	0.0282
M09	0.0319	-0.0122	-0.0174	0.0053	0.0050	0.0332
M10	0.0166	-0.0116	-0.0146	0.0019	0.0021	0.0139
M11	0.0037	-0.0024	-0.0097	0.0027	0.0030	0.0200
M12	0.0174	-0.0060	-0.0164	0.0050	0.0041	0.0247
M13	0.0424	-0.0161	-0.0127	0.0053	0.0055	0.0250
M14	0.0178	-0.0064	-0.0093	0.0022	0.0025	0.0175
M15	0.0126	-0.0143	-0.0096	0.0016	0.0018	0.0129
M16	0.0027	-0.0042	-0.0003	0.0019	0.0023	0.0137
M20	0.0016	-0.0009	-0.0011	0.0018	0.0021	0.0133
M21	-0.0045	-0.0039	-0.0009	0.0018	0.0021	0.0128

Table 1: Plane position differences are GPS derived, while height differences have derived by high precision geometric leveling (errors shown with 0.99 confidence levels).

The analyses of the vertical movements showed a similar pattern and amount of movement compared to the respective horizontal displacements. As can be seen in Figure 3 points M02, M03, M20 and M21 do not exhibit any significant vertical movement. All other points indicate a clear trend of subsidence with time, whereas point M05 represents the maximal value with 2.6 cm. The strong spatial correlation between horizontal displacements and point subsidence is pointed out in Figure 4, confirming the results obtained from the GPS field procedures and processing.

From a temporal point of view, a comparison between the subsidence values of the monitoring stations shows that all points pertaining to sector A accelerated during the first month of monitoring, with a successive deceleration for the following two weeks, and accelerated again for the rest of the monitoring period (Figure 3). Notably, a similar pattern of movement has shown the analysis of the horizontal displacements.

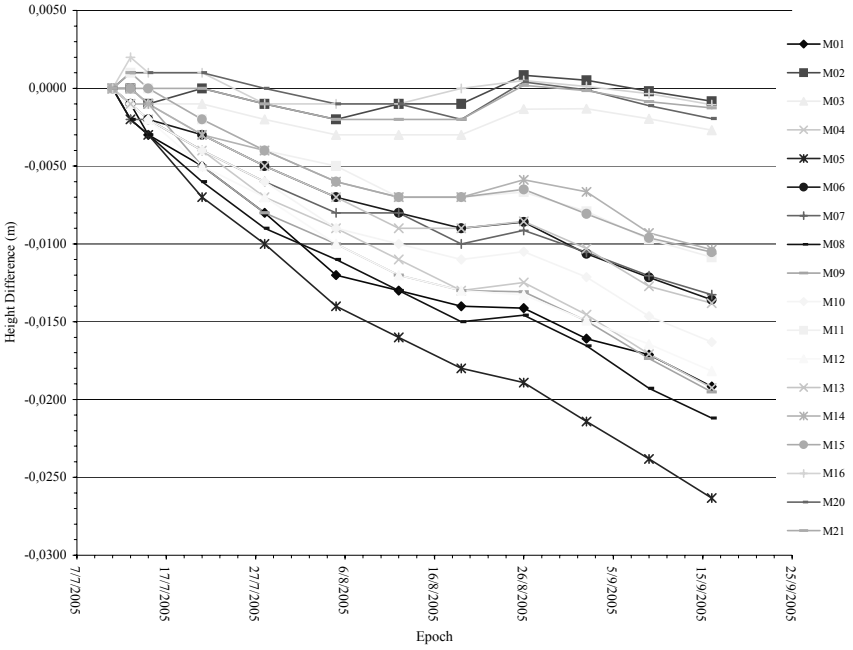

Figure 3: Cumulative vertical movement measured for every point in the entire monitoring period, taking the first observation as a reference.

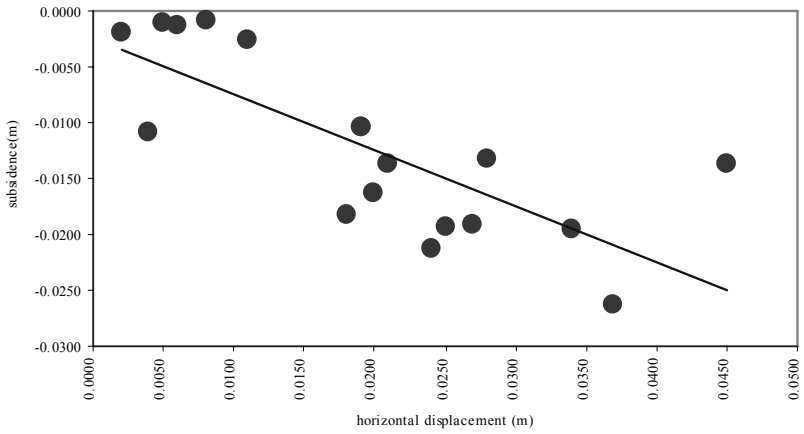

Figure 4: Horizontal displacement versus subsidence observed at every point for the period 11/07/2005 - 09/09/2005.

5. FILTERING-OUT LOCAL SLOPE GRAVITY EFFECTS

Apart from the discussion presented above regarding the origin and the causes of the planimetric position difference vectors, a more rigid approach to model and investigate them was attempted. In particular, it was assumed that the resulting differences in point positions were essentially the outcome of the local slope gravity effect and a general landslide trend common for all points of sector A, induced by the tunnel excavation. In fact, the spatial and temporal correlation overall observed in the displacement vectors analyzed in Section 3, is the sum total of a number of factors acting simultaneously on the kinematics of the landslide area. The geologic setting of the area, in common with the steepness of the ground slope could partly explain this phenomenon. On the other side, the excavation works had, undoubtedly, a serious impact on the displacement pattern depicted in Figure 2. In this study, an attempt is made in order to identify and to distinguish the observed displacement vectors into their component vectors acting primarily on the GPS stations. In essence, the model to be tested assumes that the resultant displacement observed at every point individually is the sum of two vectors described by the equation:

$$\mathrm{d}_{\mathrm{obs}_i} = \mathrm{d}_{\mathrm{local}_i} + \mathrm{d}_{\mathrm{global}} \tag{5}$$

where,

$$\mathrm{d}_{\mathrm{obs}_i} = \left[\Delta \mathrm{E}_{\mathrm{obs}_i}, \Delta \mathrm{N}_{\mathrm{obs}_i}\right]^{\mathrm{T}} \tag{6}$$

is the observed displacement vector at point i,

$$\mathrm{d}_{\mathrm{local}_i} = \left[\left|\mathrm{d}_{\mathrm{local}_i}\right| \cos\left(\frac{\pi}{2} - \mathrm{Az}_i\right), \left|\mathrm{d}_{\mathrm{local}_i}\right| \cos\left(\mathrm{Az}_i\right)\right]^{\mathrm{T}} \tag{7}$$

is the component vector that relates to slope gradient effects (i.e., gravity effects) at point i and Az is the azimuth of the slope, whereas:

$$\mathrm{d}_{\mathrm{global}_i} = \left[\Delta \mathrm{E}_{\mathrm{global}_i}, \Delta \mathrm{N}_{\mathrm{global}_i}\right]^{\mathrm{T}} \tag{8}$$

is the component vector caused by the excavation process which is assumed to be the same for every point in the network participating in the phenomenon.

In order to define in a concise way the kinematics described by this model, the number of parameters that need to be solved equals 2+n, where n is the number of points assumed to contribute in the phenomenon. More specifically, for every station in the test site, one parameter is required in order to define the length (i.e., the measure) of the component vector generated by gravity effects. In addition, two parameters are required to define the global displacement vector which is assumed to act in the same manner on every point in the network. Therefore, for a given set of points the observed displacements ℓ (2n × 1), and a vector of unknowns **x** (n+2 × 1) can be expressed by a set of observation equations, given as:

$$\ell = \mathbf{A}\mathbf{x} + \mathbf{v} \tag{9}$$

where

$$\ell = \left[\Delta \mathrm{E}_{\mathrm{obs}_1}, \Delta \mathrm{N}_{\mathrm{obs}_1}, \Delta \mathrm{E}_{\mathrm{obs}_2}, \Delta \mathrm{N}_{\mathrm{obs}_2}, \ldots, \Delta \mathrm{E}_{\mathrm{obs}_n}, \Delta \mathrm{N}_{\mathrm{obs}_n}\right]^{\mathrm{T}} \tag{10}$$

$$\mathbf{x} = \left[\Delta \mathrm{E}_{\mathrm{global}}, \Delta \mathrm{N}_{\mathrm{global}}, \left|\mathrm{d}_{\mathrm{local}_1}\right|, \left|\mathrm{d}_{\mathrm{local}_2}\right|, \ldots, \left|\mathrm{d}_{\mathrm{local}_n}\right|\right]^{\mathrm{T}} \tag{11}$$

and

$$\mathbf{A} = \begin{bmatrix} 1 & 0 & \cos\left(\frac{\pi}{2} - \mathrm{Az}_1\right) & \ldots & 0 \\ 0 & 1 & \cos\left(\mathrm{Az}_1\right) & \ldots & 0 \\ \ldots & \ldots & \ldots & \ldots & \ldots \\ 0 & 0 & 1 & 0 & \cos\left(\frac{\pi}{2} - \mathrm{Az}_n\right) \\ 0 & 0 & 0 & 1 & \cos\left(\mathrm{Az}_n\right) \end{bmatrix} \tag{12}$$

The estimated solution vector $\vec{x}$ is calculated under the minimum condition $\mathbf{v}^T\mathbf{P}\mathbf{v}$, where $\mathbf{P}$ ($2n \times 2n$) is the weight matrix of the observed displacements. If $\mathbf{P}$ is the weight matrix then following the least squares criterion the vector of parameters $\hat{\mathbf{x}}$ is given by:

$$\hat{\mathbf{x}} = \left(\mathbf{A}^T\mathbf{P}\mathbf{A}\right)^{-1}\mathbf{A}^T\mathbf{P}\ell \tag{13}$$

In this study, the kinematic model proposed by equation 4.1 was applied in the deformation data discussed in Section 3. More specifically, based on the kinematic characteristics of the GPS stations, 11 points were adopted to fulfill the model, contributing 22 observations that were processed to compute 13 unknown parameters. Figure 5 illustrates the least squares solution, in the form of a field vector that describes the global effects of motion on the GPS stations.

Clearly, this diagram shows a global trend of movement of the order of 1.9 cm over the total time span between 11/07/2005 – 09/09/2005. This global effect is pointing towards the construction site, which represents a good sign for the applicability of the model in the data. The residual analysis of the observed displacements and the computation of the unit variance of the solution verified the validity of the least squares analysis.

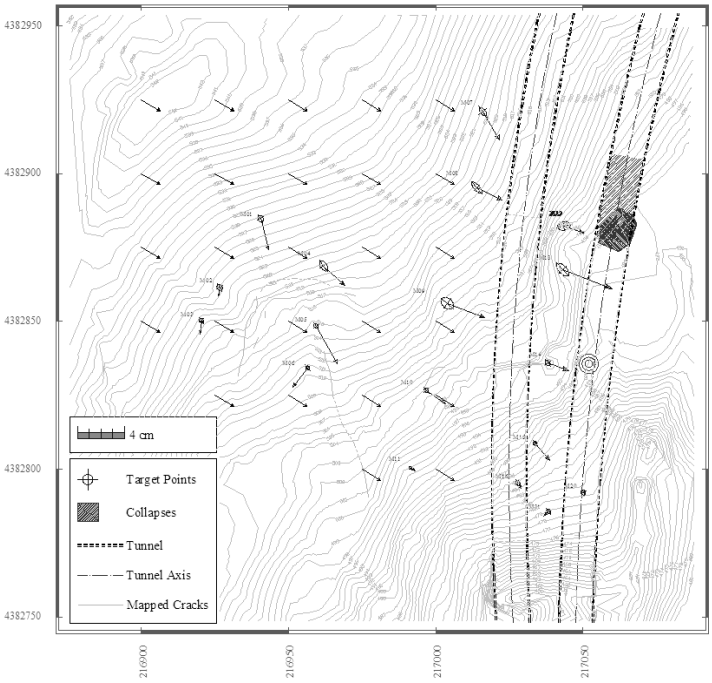

Figure 5: Image showing the relief, the tunnel, the resulting position differences at the target points and global vector field plot.

The evolution of ground deformation analyzed in this study, in common with the geologic characteristics of the area, resulted in collapses of the eastern tunnel at two locations indicated in Figure 5. By the time the last set of measurements was taken, it was decided to backfill both tunnel tubes in order to prevent against excessive roof collapse, and consequently construction has stopped. Due to the fact that monitoring has also stopped the effectiveness of the model remains to be tested, at least in this particular case.

6. CONCLUDING REMARKS

At first, and before any rigid analysis as the one presented for sector A is performed, it is clearly evident that intense plane displacements and subsidence are present with magnitudes of approximately 1.2 cm/month and 0.8 cm/month respectively. From the analysis, it is also apparent that there is a strong correlation between the direction of the plane deformations with the local slope, and a clear south-east trend, directed roughly in a fashion perpendicular to the tunnel axis.

With regard to the model which was examined to describe the kinematics of the planar deformation it can be stated that it filters-out successfully the local slope gravity effects, and thus, it isolates a global trend relating to the excavation works. However, it is advisable that this dynamic model should be tested in situations where a denser coverage with target points and/or longer monitoring time spans are available. With regard to the network design, it would be useful to install a sufficient number of target points downstream of the tunnel, as this would provide valuable information about the kinematics of the landslide, its relation to the tunneling works and the distribution of stresses in the nearby area.

References:

[1] Georgiannou, V.N.: Tunnelling Through Varying Soil Conditions in North-West Greece, Geotechnical Engineering, Issue 2, p97-104, April 2003.

[2] Lefas, I.D, Dallas, A., Power, N. Georgiannou, V.N.: Construction of Paramithia Tunnels, Egnatia Motorway, Greece, Geotechnical Engineering, Issue GE4, p197-206, October 2005.